Human Molecular Genetics, 2013, Vol. 22, No. 6 **1233–1248**
doi:10.1093/hmg/dds530
Advance Access published on December 18, 2012

Dysfunctional Coq9 protein causes predominant encephalomyopathy associated with CoQ deficiency

Laura García-Corzo[1,2], Marta Luna-Sánchez[1,2], Carolina Doerrier[1,2], José A. García[1,2], Adela Guarás[3], Rebeca Acín-Pérez[3], Javier Bullejos-Peregrín[1,2], Ana López[1,2], Germaine Escames[1,2], José A. Enríquez[3], Darío Acuña-Castroviejo[1,2] and Luis C. López[1,2,*]

[1]Instituto de Biotecnología, Centro de Investigación Biomédica, Parque Tecnológico de Ciencias de la Salud, Armilla, Granada, Spain, [2]Departamento de Fisiología, Facultad de Medicina, Universidad de Granada, Granada, Spain and [3]Centro Nacional de Investigaciones Cardiovasculares Carlos III, Madrid, Spain

Received October 21, 2012; Revised November 27, 2012; Accepted December 12, 2012

Coenzyme Q10 (CoQ_{10}) or ubiquinone is a well-known component of the mitochondrial respiratory chain. In humans, CoQ_{10} deficiency causes a mitochondrial syndrome with an unexplained variability in the clinical presentations. To try to understand this heterogeneity in the clinical phenotypes, we have generated a Coq9 Knockin (R239X) mouse model. The lack of a functional Coq9 protein in homozygous Coq9 mutant (*$Coq9^{X/X}$*) mice causes a severe reduction in the Coq7 protein and, as consequence, a widespread CoQ deficiency and accumulation of demethoxyubiquinone. The deficit in CoQ induces a brain-specific impairment of mitochondrial bioenergetics performance, a reduction in respiratory control ratio, ATP levels and ATP/ADP ratio and specific loss of respiratory complex I. These effects lead to neuronal death and demyelinization with severe vacuolization and astrogliosis in the brain of *$Coq9^{X/X}$* mice that consequently die between 3 and 6 months of age. These results suggest that the instability of mitochondrial complex I in the brain, as a primary event, triggers the development of mitochondrial encephalomyopathy associated with CoQ deficiency.

INTRODUCTION

Coenzyme Q (CoQ) biosynthesis is a complex process that is present in all mammalian tissues (1). In humans at least 11 genes codify proteins required for the biosynthesis of CoQ and have homologs in bacteria, yeast, nematodes and mice (1). One of these genes, *coq9*, was identified and characterized as a new gene that, when mutated in yeasts, results in a CoQ-deficient phenotype (2). However, the function of Coq9 protein in CoQ biosynthesis is not yet known.

Once CoQ molecules are synthesized, they localize in all tissue's membranes, thereby indicating their involvement in multiple cellular functions. Basically, all these functions are based on their redox properties. In mitochondrial inner membrane, CoQ plays a central role in the function of the mitochondrial electron transport chain (mtETC) because it is required for the transfer of electrons between complexes I and III. CoQ and its oxidation by the mtETC is also required for the function of several enzymes that link the mtETC to the function of the TCA cycle by succinate dehydrogenase (EC 1.3.5.1), to β-oxidation by the electron-transfer flavoprotein-ubiquinone oxidoreductase (EC 1.5.5.1), to the shuttling of reduction equivalents from the cytoplasm by the glycerol-3-phosphate dehydrogenase (EC 1.1.99.5), to the synthesis of pyrimidines by the dihydroorotate dehydrogenase (EC 1.3.3.1), to the metabolism of glycine by the choline dehydrogenase (EC 1.1.99.1), to the arginine and proline metabolism by the proline dehydrogenase (EC 1.5.99.8) and to the seleno-amino acid metabolism and sulfur assimilation by the sulfide CoQ reductase (EC 1.8.99.1).

Thus, CoQ is a critical molecule in the production of ATP by the mitochondrial oxidative phosphorylation (OXPHOS)

*To whom correspondence should be addressed at: Centro de Investigación Biomédica, lab 139, Universidad de Granada; Avenida del Conocimiento s/n, Armilla 18100, Granada, Spain. Tel: +34 958241000; Fax: +34 958819132; Email: luisca@ugr.es

system, which is apparently structured in mitochondrial supercomplexes (SC) that can be detected by blue native PAGE (3–5). In addition to the bioenergetics involvement, it is well known that CoQ is an important antioxidant and it participates in the redox regulation of the mitochondrial permeability transition pore and the uncoupling proteins (6).

Because of the fundamental functions of CoQ, the deficit in this vital molecule causes mitochondrial disorders with heterogeneous clinical presentations grouped in five major phenotypes: (i) an encephalomyopathy with brain involvement and recurrent myoglobinuria, (ii) an infantile multisystem disorder with encephalopathy usually associated with nephropathy and variable involvement of other organs, (iii) ataxic syndrome with cerebellar atrophy, (iv) an isolated myopathy and (v) a steroid-resistant nephrotic syndrome. Primary CoQ_{10} deficiency is transmitted as an autosomal recessive trait and may be caused by mutations in any of the known or in additional unknown genes required for its biosynthesis. To date, mutations in *PDSS1*, *PDSS2*, *COQ2*, *COQ4*, *COQ6*, *COQ9* and *ADCK3* have been identified (7). *In vitro* studies from these patients' skin fibroblasts have indicated that the decrease in mitochondrial ATP production, the increase in oxidative stress and the differences in the induction of mitophagy and apoptosis may be critical factors in the development of the disease (8–12). Nevertheless, little is known about the cellular and tissue differences in these parameters following the deficiency in CoQ levels.

To explore the molecular and pathophysiologic consequences of CoQ deficiency and the tissue-specific differences, we have generated *Coq9* knockin mouse model that develops predominant encephalomyopathy at 3 months of age. The function of the Coq9 protein in the CoQ biosynthetic pathway has also been examined.

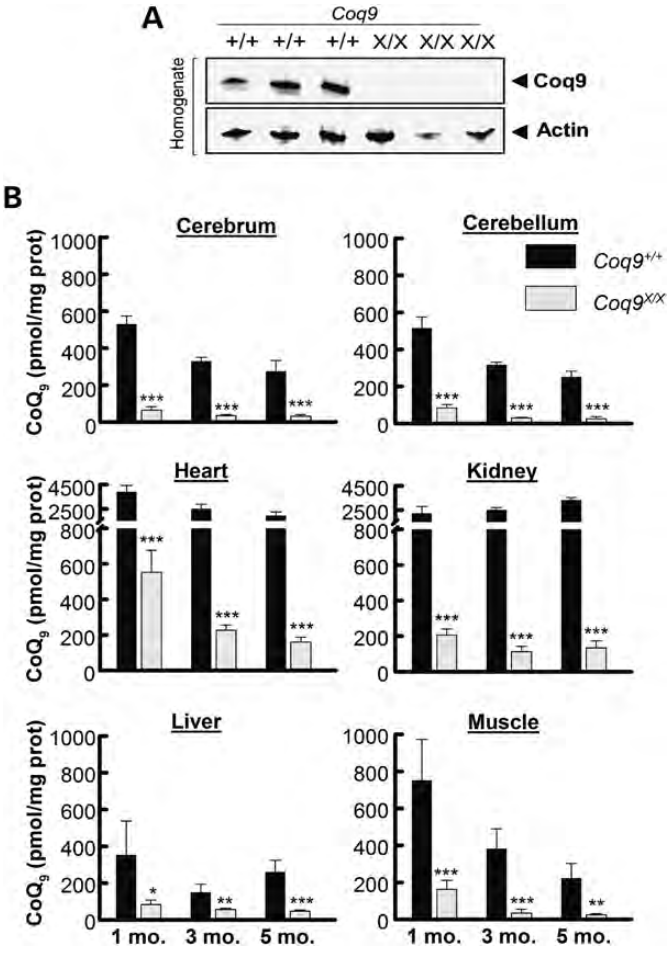

Figure 1. Mutations in the murine *Coq9* gene generate a dysfunctional Coq9 protein and a widespread CoQ deficiency. (**A**) Representative western blot analysis of Coq9 protein in heart homogenate from $Coq9^{+/+}$ and $Coq9^{X/X}$ mice. (**B**) CoQ_9 levels in tissue homogenates from $Coq9^{+/+}$ ($N = 10$) and $Coq9^{X/X}$ ($N = 10$) mice at 1, 3 and 5 months. Data are expressed as mean ± SD. $^{*}P < 0.05$; $^{**}P < 0.01$; $^{***}P < 0.005$ versus $Coq9^{+/+}$.

RESULTS

Dysfunctional Coq9 protein, which regulates Coq7, produces widespread CoQ deficiency

The *COQ9* gene was identified and characterized as a gene that is required for CoQ biosynthesis pathway in *Saccharomyces cerevisiae* (2,13). Later on, Duncan *et al.* (14) reported a patient with CoQ_{10} deficiency because of two point mutations in the *COQ9* gene. In spite of these findings, the specific role of the Coq9 protein in the CoQ biosynthesis pathway is unclear. To study the function of Coq9 in mammals, we have generated a *Coq9* mutant mouse using homologous recombination to introduce into mouse embryonic stem (ES) cells an R239X (c.715 C>T and c.717 T>A) mutation (see 'Materials and Methods' and Supplementary Material, Figs S1A–S1C) that is homologous to the human R244X *Coq9* mutation (14). Mating of heterozygous mice ($Coq9^{+/X}$) produced the expected mendelian distribution of wild-type ($Coq9^{+/+}$), heterozygous mice ($Coq9^{+/X}$) and homozygous knockin ($Coq9^{X/X}$) mice.

Murine *Coq9* gene (GenBank Accession NP_080728) comprises 9 exons on chromosome 8 and is predicted to encode a 313 amino acid protein (UniProtKB/Swiss-Prot Q8K1Z0). The $Coq9^{X/X}$ mice are predicted to produce a truncated protein lacking the C-terminal 75 amino acid residues. To confirm the presence of the truncated Coq9 protein in $Coq9^{X/X}$ mice, we first performed an immunoblotting analysis using an anti-Coq9 antibody against the C-terminal region of the protein. As predicted, we detected a ~21 kDa protein in $Coq9^{+/+}$ mice, but not in $Coq9^{X/X}$ mice (Fig. 1A). Unfortunately, an anti-Coq9 antibody against N-terminal region of the protein was not available for this study, so we could not demonstrate the presence of a stable truncated protein in $Coq9^{X/X}$ mice. Anyhow, if Coq9 is involved in CoQ biosynthesis, a dysfunctional Coq9 protein must produce a severe CoQ deficiency. As expected, $Coq9^{X/X}$ mice showed a significant decrease in both CoQ_9 (the major form of ubiquinone in rodents) and CoQ_{10} when compared with the age-mated $Coq9^{+/+}$ mice in all examined tissues (cerebrum, cerebellum, heart, kidney, hind legs skeletal muscle and liver) (Fig. 1B and Supplementary Material, Fig. S2). The percentage of decrease in both CoQ_9 and CoQ_{10} levels were slightly higher in kidney, heart, cerebrum and cerebellum, followed by muscle and liver (Supplementary Material, Table S1). Hence, our results confirmed that Coq9 protein is involved in the general pathway of CoQ biosynthesis.

An intriguing observation was that the HPLC chromatographs used to quantify the CoQ levels showed an abnormal

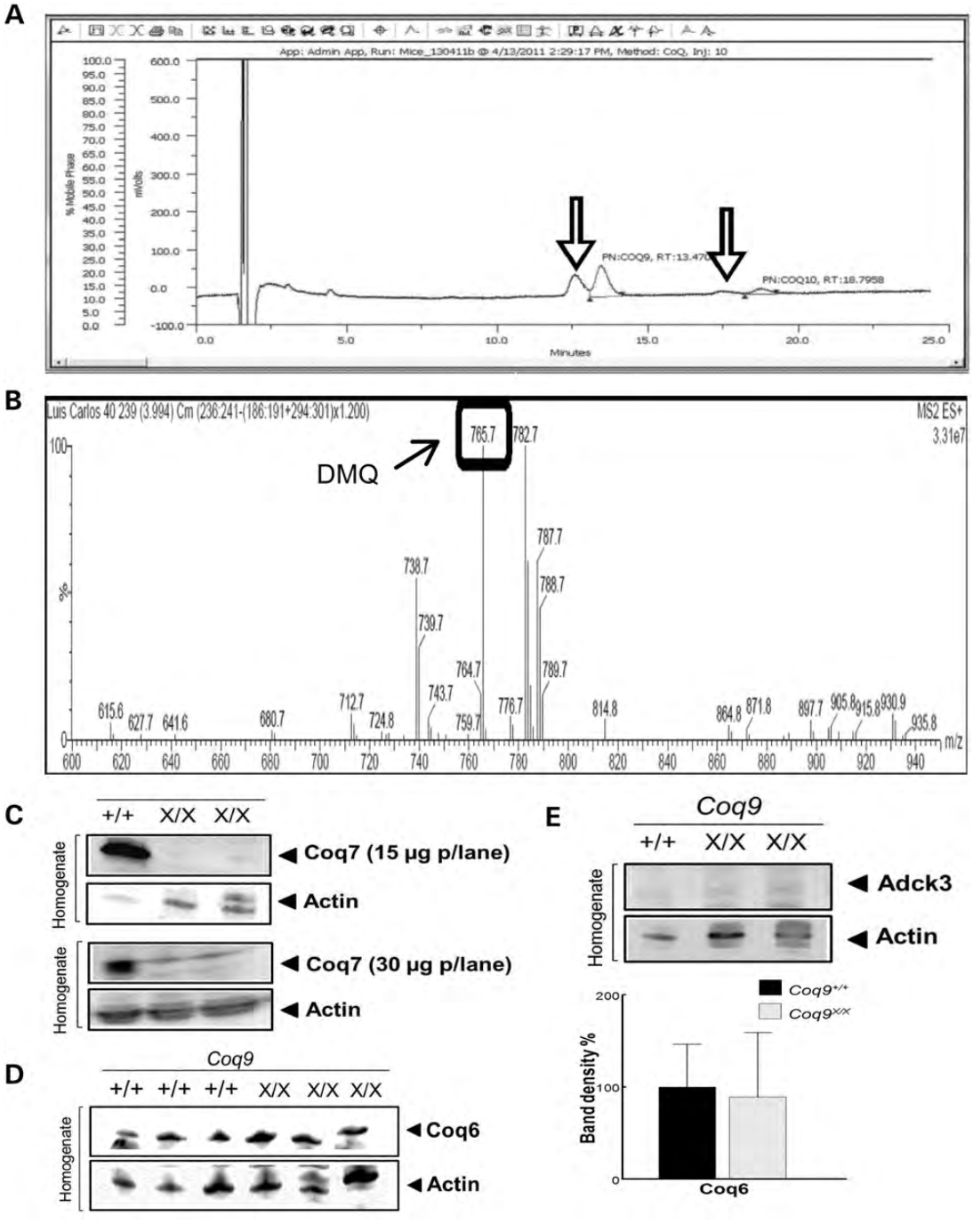

Figure 2. The role of Coq9 protein in the CoQ biosynthetic pathway. (**A**) HPLC chromatogram in the cerebrum of $Coq9^{X/X}$ mice showing two abnormal peaks at the retention times of 12.5 and 17.6 min. (**B**) Mass spectrometric analysis of the peak with a retention time of 12.5 min indicates that its molecular ion [M + H]+ corresponds to 765.7 [M + H]+. The monoisotopic mass of the precursor ion corresponds to $C_{53}H_{80}O_3 = 764.6$. This result is consistent with the identification of the abnormal peak as DMQ_9. (**C**) Protein levels of Coq7 in heart homogenate from $Coq9^{+/+}$ ($N = 6$) and $Coq9^{X/X}$ ($N = 6$) mice. The Coq7 protein was almost undetectable in $Coq9^{X/X}$ mice when 15 µg of proteins were loaded into the gel. However, low levels of Coq7 protein were detected when 30 µg of proteins were loaded in to the gel. (**D**) Protein levels of Coq6 in heart homogenate from $Coq9^{+/+}$ ($N = 6$) and $Coq9^{X/X}$ ($N = 6$) mice. The results were quantified by densitometry (right panel), and data are expressed as mean ± SD. (**E**) Protein levels of Adck3 in heart homogenate from $Coq9^{+/+}$ and $Coq9^{X/X}$ mice.

accumulation of two peaks in $Coq9^{X/X}$ mice. The retention times of these two additional peaks were 12.5 and 17.6 min, immediately before the CoQ_9 (13.5 min) and CoQ_{10} (18.8 min) peaks, respectively (Fig. 2A and Supplementary Material, Fig. S3). Interestingly, these extra peaks were also observed in the skin fibroblasts belonging to the patient with *COQ9* mutations (14). The mass spectral identification of the former lipid with a retention time of 12.5 min exhibited a molecular ion peak of 765.7 [M + H]+ (Fig. 2B) and could thus be identified as demethoxyubiquinone 9 (DMQ_9)

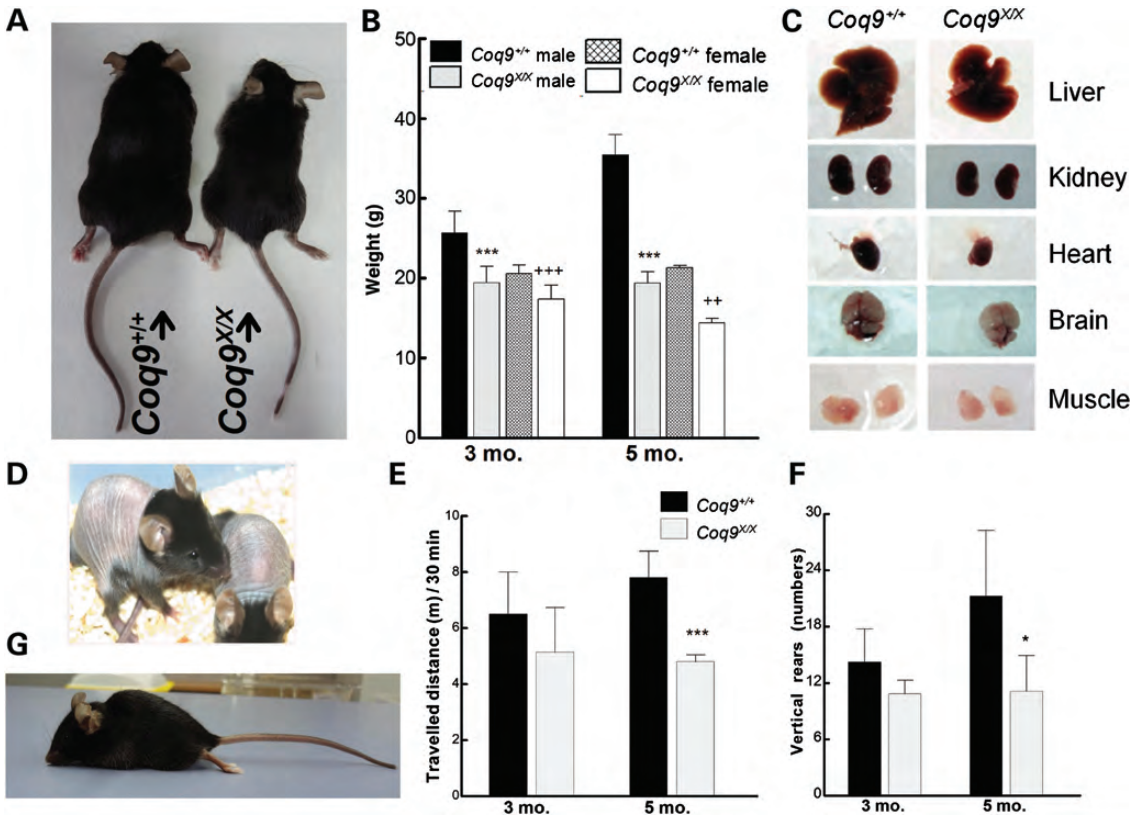

Figure 3. Phenotypic characterization of Coq9$^{X/X}$ mice. (**A**) Image of 3 months old *Coq9*$^{+/+}$ and *Coq9*$^{X/X}$ mice showing the differences in their sizes. (**B**) Body weight of males and females *Coq9*$^{+/+}$ ($N = 20$) and *Coq9*$^{X/X}$ ($N = 20$) mice at 3 and 5 months old animals. Data are expressed as mean ± SD. $^{***}P < 0.005$ versus male *Coq9*$^{+/+}$; $^{\#\#}P < 0.01$; $^{\#\#\#}P < 0.005$ versus female *Coq9*$^{+/+}$. (**C**) Image of the sizes of brain, heart, kidney, liver and muscle of *Coq9*$^{+/+}$ (left panel) and *Coq9*$^{X/X}$ mice (right panel) at 3 months of age. (**D**) Photo of a *Coq9*$^{X/X}$ mouse at 20–22nd postnatal day showing the loss of the body hair. (**E** and **F**) Open field test of *Coq9*$^{+/+}$ ($N = 16$) and *Coq9*$^{X/X}$ ($N = 16$) mice at 3 and 5 months. Traveled distance was measured by intervals of 30 min. (D) Numbers of vertical rears were evaluated by intervals of 5 min during 30 min. (E) Data are expressed as mean ± SD. $^{*}P < 0.05$; $^{***}P < 0.005$ versus *Coq9*$^{+/+}$. (**G**) Lateral view of *Coq9*$^{X/X}$ mouse with severe symptom phenotype represented by a severe paralysis of the legs.

(theoretical mass [$C_{53}H_{80}O_3$] = 764.61) (Fig. 2B). DMQ_9 was accumulated in all tissues of *Coq9*$^{X/X}$ mice, and the CoQ_9/DMQ_9 ratio was lower in kidney, heart and skeletal muscle than in cerebrum and cerebellum (Supplementary Material, Fig. S4). DMQ_9 is the substrate for the murine Coq7 protein that catalyzes its hydroxylation to produce 5-hydroxy-ubiquinone (Supplementary Material, Fig. S5). Consequently, homozygous Coq7 knockout mice accumulated DMQ_9 with no production of CoQ_9 (15,16). However, the tissues belonging to *Coq9*$^{X/X}$ mice contained both DMQ_9 and CoQ_9. Therefore, our results suggest that Coq9 may regulate Coq7. By virtue of that, we measured the protein levels of the Coq7, revealing that *Coq9*$^{X/X}$ mice showed a severe reduction in the Coq7 levels when compared with *Coq9*$^{+/+}$ mice (Fig. 2C). The reduction in the Coq7 levels in the *Coq9*$^{X/X}$ mice is very specific because the protein levels of Coq6 and Adck3 did not differ between *Coq9*$^{+/+}$ and *Coq9*$^{X/X}$ mice (Fig. 2D and E).

Coq9$^{X/X}$ mice show clinical signs of predominant encephalomyopathy

The reduction in CoQ levels in *Coq9*$^{X/X}$ mice tissues implies that this mouse model may recapitulate some of the clinical phenotypes associated with human CoQ_{10} deficiency (7). As a result, we performed an exhaustive characterization of this mouse model. *Coq9*$^{+/X}$ mice were indistinguishable from *Coq9*$^{+/+}$ mice, which corresponds with the recessive transmission of the disease (7). By crossbreeding *Coq9*$^{+/X}$ mice, a normal mendelian distribution was obtained in the offspring. *Coq9*$^{X/X}$ mice pups had normal birth weights, sex distribution and early growth. Following the first month of life, *Coq9*$^{X/X}$ mice went through a developmental delay evidenced by a reduction in the body and tissues sizes as well as in the body weight (Fig. 3A–C). Curiously, by postnatal day 20–22, the *Coq9*$^{X/X}$ mice lost their body hair (Fig. 3D), but it grew back during the next hair-growth cycle. A similar observation was provided by a complex I-deficient mouse model (17,18). Locomotor activity was lower in 3 months old *Coq9*$^{X/X}$ mice, with a significant decline at 5 months (Fig. 3E). In a similar way, the numbers of vertical rears were mildly lowered at 3 months and significantly lowered at 5 months (Fig. 3F). No differences in urine albumin, creatinine, glucose and magnesium levels were found between *Coq9*$^{X/X}$ and *Coq9*$^{+/+}$ mice (Table S2). Between 3 and 6 months, *Coq9*$^{X/X}$ mice developed a rapid and progressive leg paralysis, suggesting an involvement of the central nervous system in the pathology of the disease. In this range of age (3–6 months), *Coq9*$^{X/X}$ mice started manifesting moderate

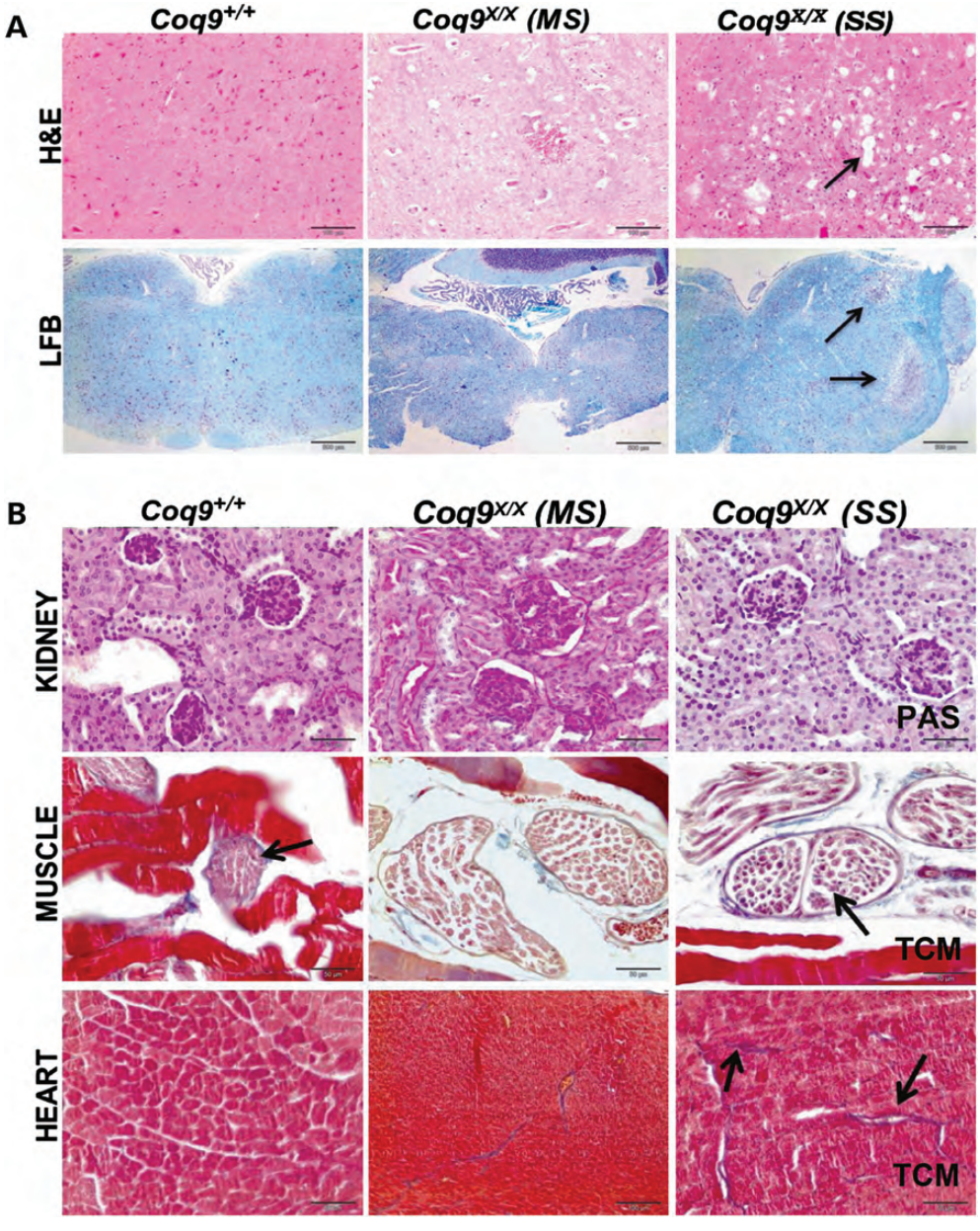

Figure 4. Histologic staining of tissue sections from $Coq9^{+/+}$ and $Coq9^{X/X}$ mice. H&E and LFB stains from $Coq9^{+/+}$ and $Coq9^{X/X}$ mice with MS and SS. A spongiform pathology is observed in $Coq9^{X/X}$ mice. The pons and the *medulla oblongata* areas show profound demyelinization in the $Coq9^{X/X}$ mice with SS (upper panel, scale bars, 100 μm; lower panel, scale bars, 500 μm). (**A**) PAS stain did not reveal histologic alterations in the kidney of both wild-type and homozygous mice (top panel and scale bar, 50 μm). The Masson's TCM stain in the muscle showed nerve fibers with severe demyelinization in $Coq9^{X/X}$ mice with SS (middle panel and scale bar, 50 μm). The heart of $Coq9^{X/X}$ mice showed an increase in connective tissue between cardiac cells (bottom panel and scale bar, 50 μm).

symptoms (MS) represented by weight loss and mild walking alterations (Supplementary Material, Movie S1) and it was followed by a progressive development of severe symptoms (SS) manifested by rapid and severe leg paralysis (Fig. 3G and Supplementary Material, Movie S2). These phenotypic changes observed in $Coq9^{X/X}$ mice were correlated with their early death: $Coq9^{X/X}$ mice started to die at 3 months, and by 4 months, 50% of them were dead. By month 6, all $Coq9^{X/X}$ mice were dead. These results suggest that $Coq9^{X/X}$ mice developed the encephalomyopathic variant associated with CoQ deficiency (7).

To determine whether the phenotype observed in $Coq9^{X/X}$ mice was the result of anatomopathologic changes, we performed a histopathologic analysis of different tissues sections. Hematoxylin and eosin (H&E) stain of the brain showed an intense vacuolization in the white matter and *medulla oblongata* from $Coq9^{X/X}$ mice, which was more evident in mice with SS. In addition, we observed dead neurons manifested by pyknotic nuclei that were displaced at the edge of the neuronal bodies (Fig. 4A). These observations indicated that $Coq9^{X/X}$ mice developed spongiform degeneration and neuronal death. Additionally, Luxol fast blue (LFB) stain revealed

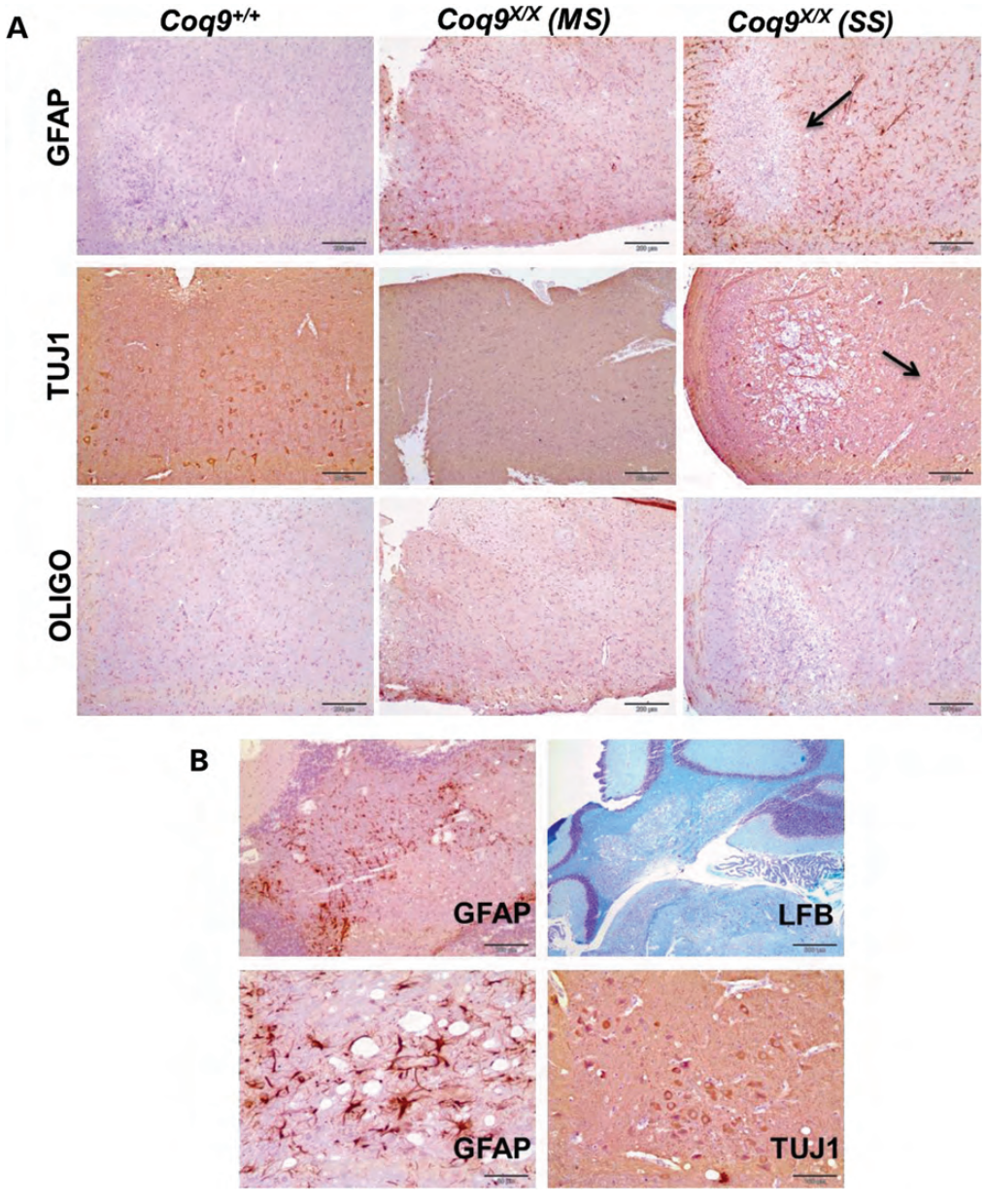

Figure 5. Histologic and inmunohistochemical staining of brain sections from *Coq9*$^{+/+}$ and *Coq9*$^{X/X}$ mice. (**A**) Anti-GFAP antibody staining of brain sections from *Coq9*$^{+/+}$, *Coq9*$^{X/X}$ (MS) and *Coq9*$^{X/X}$ (SS) mice. *Coq9*$^{X/X}$ show abnormal and striking gliotic changes evident as large numbers of GFAP immunoreactive astrocytes with large cell bodies. A clearance area in the pons is indicated with an arrow. Anti-Tubulin β-III (TUJ1) antibody staining shows a loss of neuron's dendrites in SS *Coq9*$^{X/X}$ mice. See also Supplementary Material, Figure S4A and S4B. Anti-Oligodendrocytes antibody staining did not reveal any differences between *Coq9*$^{+/+}$ and *Coq9*$^{X/X}$ mice (scale bars, 200 μm). (**B**) Anti-GFAP antibody staining and LFB staining of cerebellum of *Coq9*$^{X/X}$ mice (scale bar, 200 μm). (B) Anti-GFAP antibody staining of pons shows a reactive astrogliosis with scars formation in *Coq9*$^{X/X}$ mice with severe symptom (scale bar, 20 μm).

a profound demyelinization and an increase in glial cells in the pons and the *medulla oblongata* of *Coq9*$^{X/X}$ mice. Likewise, it is possible to distinguish a decrease in the Nissl bodies of the neurons. These changes were more evident in mice with SS (Fig. 4A). SS Masson's trichrome (TCM) stain in the hind legs skeletal muscle (*vastus lateralis*) showed nerve fibers with severe demyelinization in *Coq9*$^{X/X}$ mice (Fig. 4B). The heart showed signs of fibrosis, represented by an increase in connective tissue between cardiac cells (Fig. 4B). Finally, the Periodic acid-Schiff (PAS) stain did not reveal histologic alterations in the kidney of both wild-type and homozygous mice (Fig. 4B). In the brain, the immunohistochemistry with primary anti-glial fibrillary acid protein (GFAP) antibody revealed numerous astrocytes with enlarged cell bodies in *Coq9*$^{X/X}$ mice, particularly in the pons and cerebellum (Fig. 5A and B) and also in the encephalon. The astrocytes proliferation was more pronounced in mice with SS (Fig. 5A and B), where zones with scars formation were observed (Fig. 5B). Immunohistochemistry with primary tubulin beta III (TUJ1) antibody revealed loss of neuron's dendrites in

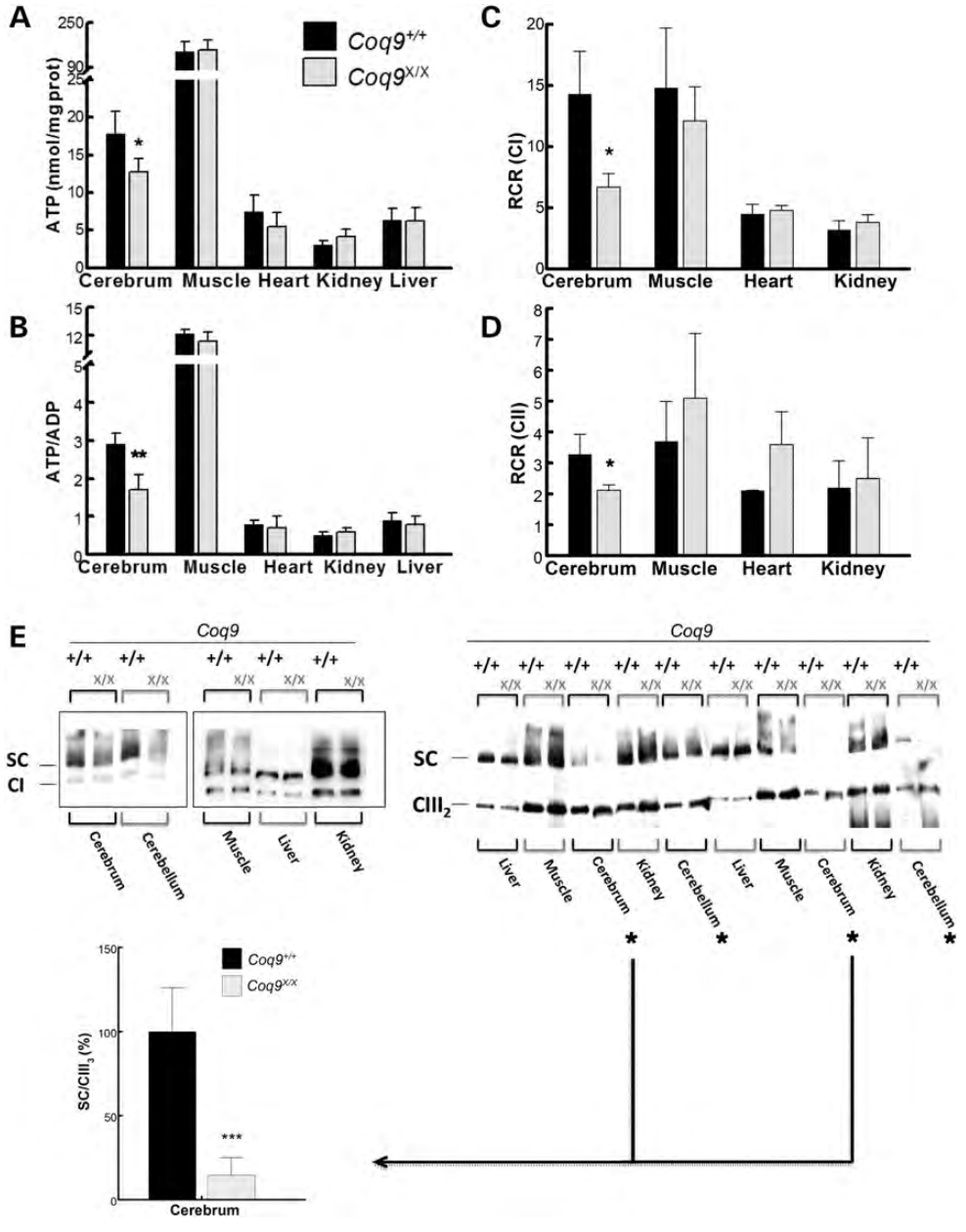

Figure 6. $Coq9^{X/X}$ mice show profound bioenergetics defect in brain. (**A** and **B**) Tissue ATP levels (A) and ATP/ADP ratio (B) from 3 months old $Coq9^{+/+}$ ($N = 7$) and $Coq9^{X/X}$ ($N = 7$) mice. Data are expressed as mean ± SD. $^{*}P < 0.05$; $^{**}P < 0.01$ versus $Coq9^{+/+}$. (**C** and **D**) Measurements of mitochondrial respiration represented by the RCR using glutamate/malate as substrates for complex I (C) or succinate as substrate for complex II (D). $N = 5$ in each experimental group. Data are expressed as mean ± SD. $^{*}P < 0.05$ versus $Coq9^{+/+}$. (**E**) BNGE followed by immunoblotting analysis of mitochondrial SC from 3 months old $Coq9^{+/+}$ ($N = 7$) and $Coq9^{X/X}$ ($N = 7$) mice. Antibodies against NDUFA9 (left panel) and Core I (right panel) were used to detect complexes I and III, respectively. Red asterisk indicate differences between $Coq9^{+/+}$ and coq9$^{X/X}$ mice. Densitometry analysis of SC and free complex III detected with the anti-core I antibody (bottom panel). Data are represented as SC/CIII ratio. The results are expressed as mean ± SD. $^{***}P < 0.005$ versus $Coq9^{+/+}$.

$Coq9^{X/X}$ mice, more evident in mice with SS (Fig. 5A and B). On the contrary, immunohistochemistry with primary anti-oligodendrocytes antibody did not show any difference between $Coq9^{+/+}$ and $Coq9^{X/X}$ mice (Fig. 5A), except for the damaged area in the pons that was not stained with any of the techniques used. Therefore, the histopathologic results in $Coq9^{X/X}$ mice showed signs of predominant encephalomyopathy with astrogliosis and neuronal death.

Defect in the mitochondrial bioenergetics correlates with the encephalomyopathic phenotype of $Coq9^{X/X}$ mice

Despite a general reduction in CoQ levels in all tissues, the more impaired organ by large in $Coq9^{X/X}$ mice is the brain. Interestingly, an analysis of the steady state level of ATP in different tissues revealed a significant decrease only in the brain (Fig. 6A). This decrease is not due to an overall decrease

in the adenine nucleotide pool but to a decrease in the ATP/ADP ratio (Fig. 6B), suggesting that the rate of ATP synthesis may be significantly impaired in the brain. Because CoQ is a key component of mitochondrial respiratory chain, the ATP depletion in the brain may reflect impairment in mitochondrial bioenergetics. The ADP-stimulated respiration (state 3) was reduced in cerebrum of $Coq9^{X/X}$ mice using substrates for both mitochondrial complex I (glutamate plus malate) (Supplementary Material, Table S3A) and complex II (succinate) (Supplementary Material, Table S3B). However, state 4 was increased using the substrates for mitochondrial complex I (Supplementary Material, Table S3A) while it was decreased using the substrate for mitochondrial complex II (Supplementary Material, Table S3B). These results suggest that respiration through complex I is partially uncoupled in cerebrum of $Coq9^{X/X}$ mice. As a consequence, the respiratory control ratios (RCRs) were significantly decreased in cerebrum of $Coq9^{X/X}$ mice (Fig. 6C and D), but the decrease in the RCR by glutamate plus malate was higher (64%) than the decrease in RCR by succinate (36%). This strongly suggests that in the brain of $Coq9^{X/X}$ mice, the complex I-dependent respiration is substantially more impaired than the complex II-dependent respiration. Mitochondria from skeletal muscle and heart of $Coq9^{X/X}$ mice showed a global reduction in oxygen consumption (Supplementary Material, Tables S3A and S3B), but no changes in the RCR (Fig. 6C and D). Kidneys of $Coq9^{X/X}$ mice did not show differences in mitochondrial respiration through complex I (Supplementary Material, Table S3A), whereas states 3 and 4 through complex II were slightly decreased (Supplementary Material, Table S3B). The RCR were not different in the kidneys from $Coq9^{+/+}$ and $Coq9^{X/X}$ mice (Fig. 6C and D). The bioenergetics defect in the cerebrum of $Coq9^{X/X}$ mice was confirmed by the measurement of the CI + III activity (Supplementary Material, Fig. S6). Moreover, the addition of decylubiquinone partially restored the CI + III activity in the cerebrum of $Coq9^{X/X}$ mice (Supplementary Material, Fig. S6).

Mitochondrial respiratory complexes could assemble into efficient supramolecular associations or SC that behave as functional and physiologic entities (4,5). Interestingly, recent studies have revealed the presence of CoQ in some SC variants (4). The analysis by blue native gel electrophoresis (BNGE) and the subsequent immunoblotting with an anti-NDUFA9 (complex I subunit) antibody showed that the overall amount of complex I substantially forming SC did not change in the mitochondria from different tissues of 3 months old $Coq9^{X/X}$ mice when compared with $Coq9^{+/+}$ mice (Fig. 6E). However, in cerebrum and cerebellum, complex I was decreased (Fig. 6E). In addition, in the immunodetection of complex III (anti-core I antibody), we observed significant differences in cerebrum and cerebellum of $Coq9^{X/X}$ mice when compared with $Coq9^{+/+}$ mice, whereas no changes in any other tissues were appreciated (Fig. 6E). Explicitly, cerebrum and cerebellum from $Coq9^{X/X}$ mice exhibited higher levels of free complex III than its form bound to the SC (Fig. 6E). This is in agreement with the reduction in complex I that would release complex III by the decrease in the amount of SC containing I/III. Therefore, the brain of $Coq9^{X/X}$ mice showed a direct correlation between the deficit in CoQ, complex I reduction, mitochondrial respiration and ATP synthesis.

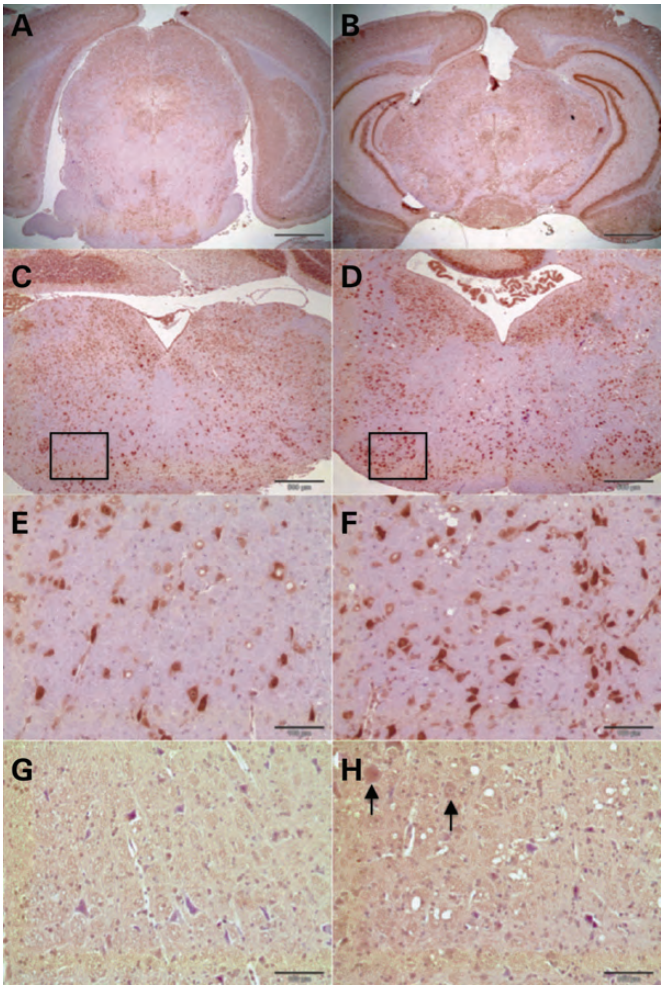

Figure 7. Oxidative damage in the brain of $Coq9^{X/X}$ mice. (**A**–**F**) Immunohistochemical stain against 8-OHdG in the brain of $Coq9^{+/+}$ (A, C and E) and $Coq9^{X/X}$ (B, D and F) mice at 3 months of age (scale bars: A and B, 1 mm; C andD, 500 μm; and E and F, 100 μm). (**G** and **H**) Immunohistochemical stain against 4-HNE in the brain of $Coq9^{+/+}$ (G) and $Coq9^{X/X}$ (H) mice at 3 months of age (scale bars, 100 μm).

Oxidative damage in the brain of $Coq9^{X/X}$ mice

Deficiencies in mitochondrial respiratory chain components are, in some cases, associated with an increase in the production of reactive oxygen species (ROS) with the subsequent oxidative damage to biomolecules. Specifically, CoQ-deficient cells have shown increased oxidative stress when the residual CoQ levels were between 30 and 45% in human skin fibroblasts (10–12) or 46 and 76% in a human neuronal cell line (19). To investigate whether the oxidative stress participates in the brain pathology of $Coq9^{X/X}$ mice, we performed an immunohistochemistry analysis of brain sections using antibodies against 8-hydroxyguanosine (8-OHdG), a marker of nucleic acid oxidation, and 4-hydroxynonenal (4-HNE), a marker of lipid peroxidation. $Coq9^{X/X}$ mice showed an increased number of positive cells for 8-OHdG (Fig. 7A and B) and increased intensity in the staining, which is especially evident in the pons (Fig. 7C–F). The immunostaining against 4-HNE did not show profound differences between

Coq9$^{+/+}$ and *Coq9*$^{X/X}$ mice. However, some neurons in the encephalon of *Coq9*$^{X/X}$ mice showed an increase in 4-HNE stains (Fig. 7G and H).

The energy deficit in neurons triggers caspase-independent apoptosis

Defects in the mitochondrial function are the more plausible explanation for the impossibility of brain tissue to maintain normal levels of ATP. This energetic failure may cause neuronal death and be the primary cause of the histopathologic features on *Coq9*$^{X/X}$ mice. In fact, the histologic study of the brain showed the presence of dead neurons in the Coq9$^{X/X}$ mice with SS. To verify how neuronal death occurred, we performed the TUNEL assay in different brain sections. Brain images of *Coq9*$^{X/X}$ mice with MS did not reveal the presence of apoptotic neurons (Fig. 8A). However, brain images from *Coq9*$^{X/X}$ mice with SS revealed the presence of apoptotic cells in the pons and in the encephalon (Fig. 8A). Following that, we investigated the mechanisms by which apoptosis was developed. First, we detect low levels of caspase 3 and p53 in mutant mice, as well as overexpression of the antiapoptotic protein bcl2 (Fig. 8B), implying that a caspase-dependent cell death pathway was not activated. Intrigued by our finding that pointed to an apoptotic process in the cerebrum of the *Coq9*$^{X/X}$ mice, we measured the expression of the apoptosis induction factor (AIF) in this tissue to check whether a caspase-independent cell death pathway was activated. Interestingly, we found a significant translocation of AIF from the mitochondria to the nucleus suggesting that the apoptotic process triggered was in fact a caspase-independent pathway (Fig. 8C).

DISCUSSION

Following the first reports of human CoQ_{10} deficiency, there has been an increased interest in discovering the different steps and regulation aspects of CoQ biosynthetic pathway, as well as the pathomechanisms associated with CoQ_{10} deficiency. In the current study, the generation and characterization of *Coq9*$^{X/X}$ mice favor some important conclusions regarding these inquiries: (i) Coq9 protein specifically regulates Coq7 protein in the CoQ biosyhthetic pathway, (ii) the presence of a dysfunctional Coq9 protein and/or the deficit in CoQ in the brain causes loss of complex I and an increase in free complex III, leading to a decrease in mitochondrial respiration and ATP synthesis, (iii) mitochondrial dysfunction in the brain induces a caspase-independent apoptotic cell death and (iv) the encephalomyopathic form of CoQ deficiency is progressive and takes place with neuronal death, severe reactive astrogliosis and spongiform degeneration.

CoQ biosynthesis is a complex process that is known in part, thanks to research in bacteria and yeast. One of the proteins involved in this biosynthetic pathway is Coq9, but its specific function is unknown. The involvement of Coq9 in CoQ biosynthesis was initially discovered in yeasts because *coq9* mutant yeasts did not produce CoQ_6 (2). Interestingly, *coq9* point mutant yeasts harboring *adck3* (*coq8*/*abc1*) on a multicopy plasmid have partial CoQ_6 biosynthesis and accumulation of DMQ_6 (2,20). *Coq9*$^{X/X}$ mice have constitutive levels of Adck3, and they show, similar to *coq9* point mutant yeasts harboring *adck3* on a multicopy plasmid (2,20), reduced CoQ_9 levels and accumulation of DMQ_9. Because DMQ_9 is the substrate for the reaction catalyzed by Coq7, we hypothesized that Coq7 may require Coq9 for its normal function. The reduced levels of Coq7 together with the normal levels of Coq6 and Adck3, other enzymes in the CoQ biosynthesis, confirmed this premise. Coq9 protein has no homology with proteins of known function, but the prediction indicates that it works as a cation/ion/metal-binding protein (Kihara Bioinformatics Laboratory, IN, USA). Because Coq7 possess a di-iron center (21), we may speculate that Coq9 is necessary for the proper conformation of this di-iron center in the Coq7 protein. The co-localization of Coq7 and Coq9 in rat molecular podocytes would reinforce this idea (22).

Once CoQ molecules are synthesized, they play a central role in the OXPHOS system transferring electrons from complexes I and II to complex III (3,23). The OXPHOS system is organized into efficient supramolecular associations or SC. Interestingly, Acín-Pérez and *et al.* (24) demonstrated that complex I, almost in its totality, is forming physical association with complex III *in vivo* to the point that the ablation of complex III destabilizes complex I and promotes its degradation. It is also described that the depletion of complex I does not disestablish complex III, but modifies its distribution between free and supercomplex-associated complex III (24). *Coq9*$^{X/X}$ mice showed reduction in complex I with a parallel increase in free complex III only in the brain. This reduction in the complex I amount correlates with the partial restoration of the CI + III activity after the addition of decylubiquinone. In other CoQ-deficient tissues with stable mitochondrial I/III ratios, no differences in mitochondria coupled respiration and ATP levels were found between *Coq9*$^{+/+}$ and *Coq9*$^{X/X}$ mice. Therefore, our study suggests that the destabilization of the mitochondrial complex I is a critical event triggered by the CoQ deficiency that reduces mitochondrial ATP synthesis. It is unclear why this tissue has a specific defect, but the differences (~40%) in the protein composition of mitochondria from different mouse tissues suggest that there are differences in the mitochondria organization and function depending on the tissue (25). One possibility is a tissue-specific role of Coq7, which is reduced in the *Coq9*$^{X/X}$ mice, in the distribution of CoQ through the outer and inner mitochondrial membranes, as it has been recently suggested (26). Therefore, further investigations will be needed to clarify whether the loss of complex I in brain is a molecular-specific or CoQ levels-specific phenomenon.

The accumulation of DMQ_9 in *Coq9*$^{X/X}$ mice tissues does not seem to be a critical factor for the cerebrum-specific bioenergetics impairment because cerebrum and cerebellum showed higher CoQ_9/DMQ_9 ratios than other tissues. DMQ is not functional in the mitochondrial respiratory chain, (27) and mice with accumulation of DMQ_9 and no production of CoQ are embryonically lethal (15,16). Moreover, the accumulation of DMQ does not seem to produce detrimental effects in the mitochondrial respiratory chain because Coq9 and Coq7 mutant yeasts are not functionally distinguishable from other ubiquinone-deficient mutant yeasts (1,28).

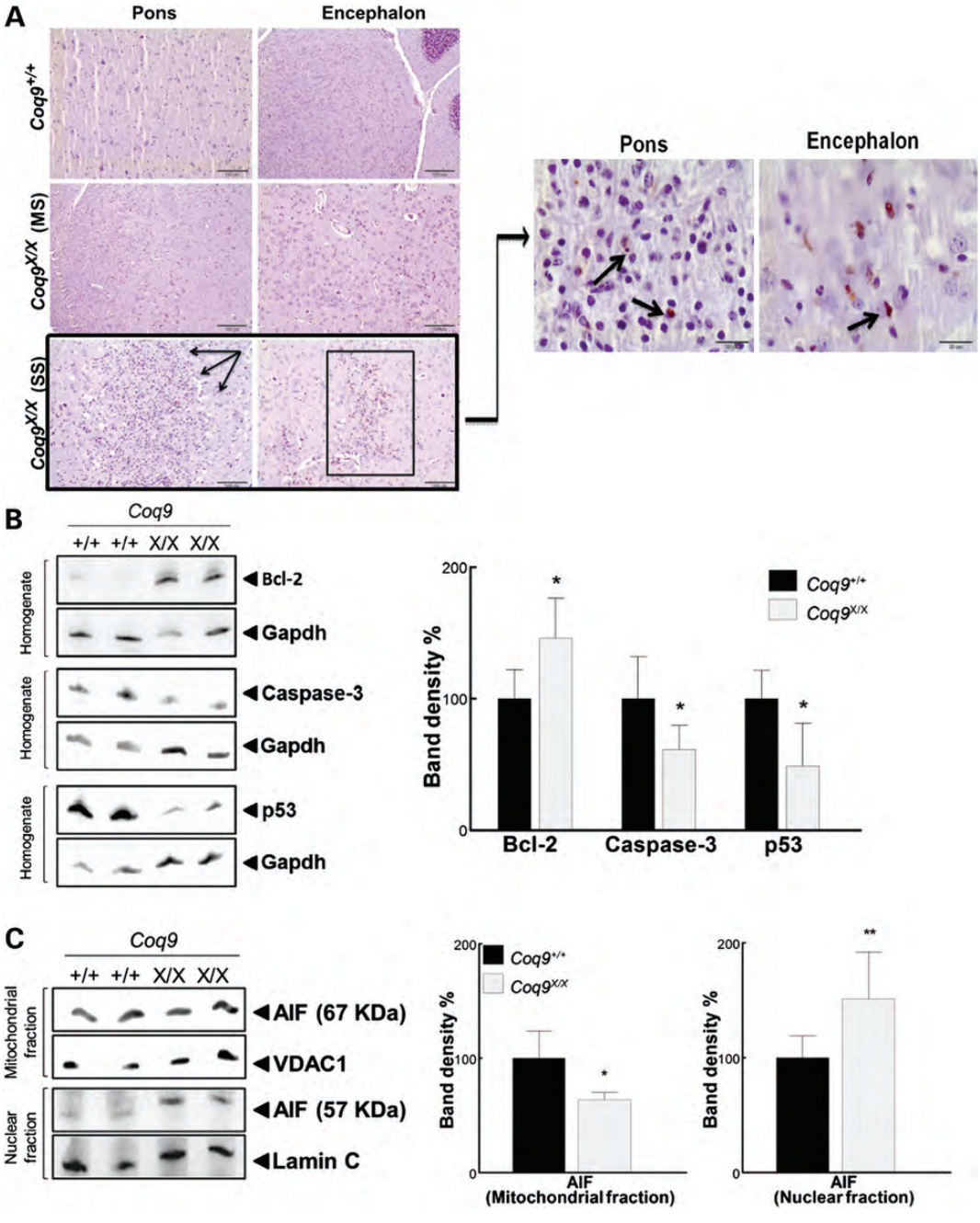

Figure 8. Apoptotic markers in the brain of $Coq9^{+/+}$ and $Coq9^{X/X}$ mice. (**A**) Pons and encephalon from $Coq9^{+/+}$, $Coq9^{X/X}$ (MS) and $Coq9^{X/X}$ (SS) mice stained by the TUNEL assay. Apoptotic bodies were detected in both areas from $Coq9^{X/X}$ (SS) mice (scale bars, 100 μm). (**B**) Analysis of the caspase-dependent mitochondrial apoptotic pathway in cerebrum of $Coq9^{+/+}$ ($N = 7$) and $Coq9^{X/X}$ ($N = 7$) mice. The results were quantified by densitometry (right panels), and data are expressed as mean ± SD. $^{*}P < 0.05$ versus $Coq9^{+/+}$. (**C**) Analysis of the caspase-independent mitochondrial apoptotic pathway in cerebrum of $Coq9^{+/+}$ ($N = 7$) and $Coq9^{X/X}$ ($N = 7$) mice. The results were quantified by densitometry (bottom panel), and data are expressed as mean ± SD. $^{*}P < 0.05$; $^{**}P < 0.01$ versus $Coq9^{+/+}$.

The consequence of energy depletion in the brain is an increase in apoptotic neuronal death triggered by translocation of AIF from mitochondria to the nucleus, a route of cell death pathway mitochondrial dependent, but caspase independent. The AIF-dependent pathway seems to be particularly important in the induction of apoptosis in neurons (29–31). Similar to our results, the cell death induced as a consequence of the lack of mitochondrial glutathione peroxidase 4 (GPx4) was mediated through the AIF translocation to the nucleus (31). Moreover, caspase 3 was not activated in the $GPx4^{-/-}$ cells, and the overexpression of Bcl2 did not prevent the apoptosis cell death (31). Similar outcomes were found in the brain of $Coq9^{X/X}$ mice. Another question, however, is whether the energy depletion is the only cause of the caspase-independent cell death. In this regard, the cell death in CoQ_{10}-deficient fibroblasts has been associated with a combination of

increased oxidative stress and a decreased ATP synthesis (11,32). Takahashi and *et al.* (33) suggested that the increase in apoptosis in the embryos of *Coq7* knockout mice was caused by the bioenergetics failure. Other important issue is that the mechanisms to induce apoptosis may be different depending on the cell type or tissue. In cortical neurons, for example, it has been suggested that both energy failure and oxidative stress would contribute to the caspase-independent neuronal death (34). This circumstance may be also plausible in the brain of $Coq9^{X/X}$ mice, where an overall increase in 8-OHdG and accumulation of 4-HNE in some neurons were observed. The increased oxidative damage detected in the brain of $Coq9^{X/X}$ mice and in the kidney of *Pdss2* mutant mice suggests that oxidative stress is involved in the pathology of CoQ deficiency *in vivo* (35,36). Future studies with an exhaustive evaluation of the ROS generation, oxidative damage and antioxidant defenses in $Coq9^{X/X}$ mice tissues, as well as the effects of antioxidant therapies, will provide the detailed mechanisms of the induction of the caspase-independent neuronal death.

Finally, the histopathologic evaluation of $Coq9^{X/X}$ mice showed loss of neuronal dendrites and neuronal death, demyelinization in the white matter and the ponds of the brain, as well as in the nerve fibers of the hind leg skeletal muscle, and signs of fibrosis in the heart. The neuronal death also induced reactive astrogliosis, a process that can exert beneficial effects in the initial phase, supporting neuronal survival; however, when the response progresses over time, the reactive astrogliosis may be detrimental (37). This last phase of reactive astrogliosis can be identified by a typical scar formation that is clearly apparent in the brain of $Coq9^{X/X}$ mice with SS.

The causes of the clinical heterogeneity associated with human CoQ_{10} deficiency are poorly understood. The main progress in this area has been developed in cellular models because of the lack of suitable animal models with the different clinical phenotypes. The $Coq9^{X/X}$ mice described here is the first animal model showing biochemical, molecular, histologic and behavioral signs resembling human mitochondrial encephalomyopathy associated with CoQ deficiency. The tissue-specific pathomechanisms described in $Coq9^{X/X}$ mice unlock new possibilities for the mitochondrial organization and function. Given that some of these mechanisms are common to other mitochondrial encephalomyopathies as well as neurodegenerative and neuromuscular disorders, this $Coq9^{X/X}$ mouse model will be very useful not only for developing and testing therapies for CoQ deficiency but also for other illnesses related to mitochondria.

MATERIALS AND METHODS

Generation of knockin Coq9 mouse

A positively identified C57BL/6 BAC clone, RP23-128L6, was used to isolate the Coq9 genomic sequence for vector construction. A 7.72 kb fragment spanning from the upstream of exon 4 to downstream of exon 9 was first subcloned into a backbone vector derived from vector plasmid pSP72 (Promega) using the recombineering technology. The mutation CGT > TGA (R239X) within exon 7 was generated by three-step PCR mutagenesis. Four mutagenesis primers [PT1, PT2, PT3 and PT4 (*BsiWI*)] were designed to amplify a fragment with the size of 1165 bp, which incorporates the mutation at the desired location (Supplementary Material, Fig. S1A). The PCR fragment containing the mutation was then used to replace the wild-type sequence using an endogenous *Eco*RV site and an engineered *Bsi*WI site. The neomycin drug selection cassette flanked by both LoxP and flippase recognition target (FRT) sites is inserted 205 bp downstream of exon 7. The final targeting vector is composed of a long homology arm extending ~5.2 kb 5′ to the point mutation in exon 7, a short homology arm extending 2.17 kb 3′ to the neomycin cassette, the engineered mutation Arg > stop and the neomycin selection cassette flanked by LoxP and FRT sites (Supplementary Material, Fig. S1B). The total size of the targeting construct (including the backbone vector) is 11.82 kb. It contains both ampicillin- and kanamycin- resistant genes for bacteria transformation. The targeting vector was confirmed by restriction analysis and sequencing after each modification. The vector was linearized by *Not*I restriction enzyme digestion and then transfected into IC1 C57BL/6 ES cells by electroporation to generate targeted ES cell lines (inGenious Targeting Laboratory, NY, USA).

After selection with G418 antibiotic, approximately 200 resistant clones were isolated and screened by PCR using *Coq9* primers outside of the targeting sequence with neomycin-resistant gene primers. Homologous recombinants were confirmed by Southern blot analyses using probes recognizing *Coq9* genomic sequences outside of the targeting vector (Supplementary Material, Fig. S1C) (primers A1, LAN1, COOK3 and UNI). Presence of the c.715 C>T and c.717 T>A mutations were confirmed by sequencing (primer COOK4). Cells from two to four ES clones harboring the homologous recombinants were submitted for injection into C57BL/6J blastocysts and generation of chimeric mutant mice. The germline transmission of the mutation was confirmed by PCR, Southern blot (Supplementary Material, Fig. S1D) (primers PT1, F7, A1 and F3) and sequencing (primer COOK4). Heterozygous mice were subsequently bred with FLPe mice (38) on a C57BL/6 background to remove the Neo cassette. The deletion of the Neo cassette was confirmed by PCR using the Neo Del1 and Neo Del2a primers. The FLPe transgene was eventually eliminated from the pedigree by further breeding. For all experiments, heterozygous mice for the knockin allele were crossbreed to obtain wild-type controls ($Coq9^{+/+} = Coq9^{+/+}$), heterozygous knockin ($Coq9^{+/R239X} = Coq9^{+/X}$) or homozygous knockin ($Coq9^{R239X/R239X} = Coq9^{X/X}$) mice. Mice were housed in the Animal Facility of the University of Granada under an SPF zone with lights on at 7:00 am and off at 7:00 pm. Mice had unlimited access to water and rodent chow. Institutional Animal Care and Use Committees approved all experiments.

Quantification of CoQ_9 and CoQ_{10} levels in mice tissues

CoQ_9 and CoQ_{10} from mice tissues were extracted by mixing tissue extracts with 1-propanol. After 2 min vortex, the solution was centrifuged at 11 300 *g* for 5 min. The resultant supernatant was injected in a HPLC system (Gilson, WI, USA), and the lipid components were separated by a reverse phase symmetry C18 3.5 μm, 4.6 × 150 mm column (Waters, Spain), using a mobile phase consisting of methanol,

ethanol, 2-propanol, acetic acid (500:500:15:15) and 50 mM sodium acetate at a flow rate of 0.9 ml/min. The electrochemical detector consisted of an ESA Coulochem III with the following setting: guard cell (upstream of the injector) at +900 mV, conditioning cell at −600 mV (downstream of the column) and followed by the analytical cell at +350 mV (32). CoQ_9 and CoQ_{10} concentrations were estimated by comparison of the peak areas with those of standard solutions of known concentrations. The results were expressed in pmol CoQ/mg protein.

Ultra carrying out liquid chromatography- mass spectrometer (MS/MS) analysis of intermediate metabolites

Lipids extracts were obtained as described above for the CoQ quantification. Samples were analyzed using an Acquity ultra carrying out liquid chromatography system coupled to a Xevo TQS detector of mass spectrometer (MS/MS) with an electrospray ionization (Waters Corporation). The analytical separation column was a BEH C18, 1.7 μm, 2.1 × 50 mm column (Waters, Spain) (39). The mobile phase consisted of methanol and 5 mM ammonium acetate at the constant flow rate of 0.3 ml/min. Source and desolvation temperatures were set at 150 and 300°C, respectively. Nitrogen was used as both cone gas (150 l/h) and desolvation gas (500 l/h), and argon was used as collision gas (0.14 ml/min). Mass spectrometry analyses were carried out in full scan mode between 600 and 950 uma to improve the sensitivity of the analysis.

Evaluation of SC formation by BNGE

BNGE was performed on mitochondrial fraction from mice tissues. Mitochondrial isolation was performed as previously described (40). Tissues were homogenized in a glass–teflon homogenizer. Liver and kidney were homogenized (1: 4, w/v) in the homogenization medium A [0.32M sucrose, 1 mM EDTA and 10 mM Tris–HCl (pH 7.4)]; cerebrum and cerebellum were homogenized (1:5, w/v) in the homogenization medium A plus 0.2% free fatty acids BSA; heart was homogenized (1:10, w/v) in the homogenization medium B [0.075 M sucrose, 0.225 M sorbitol, 1 mM ethylene glycol tetraacetic acid (EGTA), 0.1% free fatty acids BSA, 10 mM Tris–HCl (pH 7.4)]; and skeletal muscle was homogenized (1:20, w/v) with ultraturex in homogenization medium C (0.12 M KCl, 0.02 M 4-(2-hydroxyethyl)-1-piperazineethanesulfonic acid (HEPES), 2 mM $MgCl_2$, 1 mM EGTA and 5 mg/ml free fatty acids BSA). Liver, kidney, cerebrum, cerebellum and heart homogenates were centrifuged at 1000*g* for 5 min at 4°C to remove nuclei and debris. Mitochondria were collected from supernatants after centrifuging at 14 400*g* for 2 min at 4°C. Skeletal muscle homogenate was centrifuged at 600*g* for 10 min at 4°C. The supernatant (s1) was kept on ice, and the pellet was re-suspended in eight volumes of buffer A and centrifuged at 600*g* for 10 min at 4°C. The subsequent supernatant (s2) was combined with s1 and centrifuged at 17 000*g* for 10 min at 4°C. The pellet obtained was re-suspended in 10 volumes of medium A and centrifuged at 7000*g* for 10 min at 4°C. The pellet was re-suspended in one volume of medium B (0.3 M sucrose, 2 mM HEPES and 0.1 mM EGTA) and centrifuged at 3000*g* for 10 min at 4°C.

The mitochondrial pellets from all tissues were suspended in 75 μl (heart and cerebellum), 120 μl (skeletal muscle), 140 μl (cerebrum and kidney) and 800 μl (liver) in the corresponding homogenization buffers. An aliquot of each sample was used for protein determination. The remaining samples were then centrifuged at 17 000*g* for 3 min at 4°C. Mitochondrial pellets were suspended in an appropriate volume of buffer D [1 M 6-aminohexanoic acid, 50 mM Bis–Tris–HCl (pH 7.0)] to be at 10 mg/ml, and the membrane proteins were solubilized by the addition of digitonin (4 g/g) and incubated for 5 min in ice. After 30 min of centrifugation at 13 000*g*, the supernatant was collected, and 3 μl of 5% Brilliant Blue G dye prepared in 1 M 6-aminohexanoic acid was added (4). Mitochondrial proteins (100 μg) were then applied and run on a 3–13% gradient native gel using electrophoresis system mini-PROTEAN Tetra Cell (Bio-rad). Western blot was performed using a mini Trans-blot Cell onto polyvinylidene difluoride membranes and probes with specific antibodies against complex I, anti-NUDFA9 (Abcam, ab14713) and complex III, anti-ubiquinol-Cytochrome C Reductase Core Protein I (Abcam, ab110252) (4).

Sample preparation and western blot analysis

Western blot analyses were performed in cerebrum and heart homogenates, as well as mitochondrial and nuclei fractions. For the experiments in total homogenate samples, cerebrum and heart were homogenized in homogenization buffer A (50 mM Tris–HCl, 1% Triton X-100 and 1 mM Dithiothreitol, pH 7.6, protease inhibitor cocktail) at 1100 r.p.m in a glass–teflon homogenizer. Tissue homogenate was sonicated and centrifuged at 1000*g* for 5 min at 4°C, and the resultant supernatant was used for western blot analysis. For mitochondria isolation, the cerebrum was homogenized in homogenization buffer B (0.32 M sucrose, 10 mM Tris–HCl, 1 mM EDTA and 0.2% fatty acid-free BSA, pH 7.4, protease inhibitor cocktail) at 600 r.p.m in a glass–teflon homogenizer. Cerebrum homogenate was centrifuged at 1000*g* for 5 min at 4°C. The supernatant was then centrifuged at 17 000*g* for 2 min at 4°C. The resultant pellet containing the mitochondrial fraction was washed in 1.5 ml of homogenization buffer B under similar conditions. The mitochondrial pellet was re-suspended in 100 μl of homogenization buffer A and stored in aliquots at −80°C. For nuclei isolation, cerebrum was excized, weighed, washed with saline and homogenized in 0.5 ml phosphatase inhibitor buffer (10 mM phosphate buffer, 150 mM NaCl, 2.7 mM KCl, 125 mM NaF, 250 mM β-glycerophosphate, 250 mM *p*-nitrophenyl phosphate and 25 mM $NaVO_3$, pH 7.5) at 600 r.p.m with a Stuart Scientific SS2 stirrer with a teflon pestle. The homogenate was centrifuged at 300*g* for 5 min at 4°C, and the pellet obtained was re-suspended in 0.25 ml of ice-cold hypotonic buffer (20 mM HEPES, pH 7.5, 5 mM NaF, 5 μl of 0.1 M Na_2MoO_4 and 0.1 mM EDTA). After incubation for 15 min at 4°C, 50 μl of 10% IGEPAL was added, and the sample was then centrifuged at 14 000*g* for 1 min at 4°C. The nuclear pellet was re-suspended in 100 μl of lysis buffer (20 mM HEPES, pH 7.9, 20% glycerol, 420 mM NaCl, 1.5 mM $MgCl_2$, 0.2 mM EDTA, 20 mM NaF, 0.5 mM dithiothreitol, 1 μg/ml leupeptin and 0.2 mM phenylmethylsulfonyl

fluoride), followed by incubation at 4°C for 30 min on a shaking platform. After vortex mixing, the resulting suspension was centrifuged at 14 000*g* for 10 min at 4°C. The supernatant (nuclear fraction) was stored in aliquots at −80°C (41).

Fourteen micrograms of proteins from the sample extracts were electrophorezed in a PhastGel™ Homogeneous 12.5 using a PhastSystem instrument (GE Healthcare Europe GmbH, Spain). The proteins were transferred to an Amersham Hybond™ ECL™ nitrocellulose membrane (GE Healthcare Europe GmbH, Spain) and probed with target antibodies. Protein–antibody interactions were detected with peroxidase-conjugated horse anti-mouse, anti-rabbit or anti-goat IgG antibodies (Santa Cruz Biotechnology, Inc.), using Amersham ECL™ prime western blotting detection reagent (GE Healthcare Europe). Bands quantification were carried out using an Image Station 2000R (Kodak, Spain) and the Kodak 1D 3.6 software. Quantitative values of the bands were normalized by GAPDH, actin, β-actin, VDAC1 or Lamin C, and the data were expressed in terms of percent relative to wild-type mice.

The following primary antibodies were used: anti-COQ7 (generously provided by Dr Hekimi, McGill University, Canada), anti-COQ6 (Santa Cruz Biotechnology, sc-107506), anti-COQ9 (Santa Cruz Biotechnology, sc-271892), anti-COQ9 (Abcam, ab104189), anti-NRF-1 (Santa Cruz Biotechnology, sc-33771), anti-PGC-1α (Santa Cruz Biotechnology, sc-13067), anti-Bcl-2 (Santa Cruz Biotechnology, sc-492), anti-caspase-3 (Santa Cruz Biotechnology, sc-136219), anti-p53 (Santa Cruz Biotechnology, sc-6243) and anti-AIF (Santa Cruz Biotechnology, sc-55519). As loading controls, the following antibodies were used: anti-β-actin (Santa Cruz Biotechnology, sc-47778), anti-GAPDH (Santa Cruz Biotechnology, sc-25778), anti-Actin (Santa Cruz Biotechnology, sc-1616), anti-VDAC1 (Abcam, ab14734) and anti-Lamin A/C (Santa Cruz Biotechnology, sc6215).

Mitochondrial respiration

To isolate fresh mitochondria, mice were sacrificed, and the organs were extracted rapidly on ice. Muscle and heart were submerged in 1 mg/ml proteinase K solution (for 30 s in heart and 60 s in hind leg skeletal muscle). Then, tissues were homogenized (1:10, w/v) in isolation buffer (250 mM sucrose, 2 mM EDTA, 10 mM Tris and 0.5% free fatty acids albumin, pH 7.4) at 800 r.p.m at 4°C with a glass–teflon homogenizer. The homogenate of each tissue was centrifuged twice at 1000*g* for 5 min at 4°C, and the supernatant was centrifuged at 23 000*g* for 10 min at 4°C. Then, the mitochondrial pellets were suspended in 1 ml of isolation buffer and centrifuged at 13 000*g* for 3 min at 4°C. The final crude mitochondrial pellet was re-suspended in MiR05 medium [0.5 mM EGTA, 3 mM $MgCl_2$, 20 mM Taurine, 10 mM KH_2PO_4, 20 mM Hepes, 110 mM D-sucrose, 60 mM lactobionic acid and 0.1% (w/v) free fatty acid albumin, pH7]. Kidney was homogenized (1:10, w/v) in a respiration buffer A (250 mM Sucrose, 0.5 mM Na_2EDTA, 10 mM Tris and 1% free fatty acid albumin) at 800 r.p.m in a glass–teflon homogenizer. Then, the homogenate was centrifuged at 500*g* for 7 min at 4°C, and the supernatant was centrifuged at 7800*g* for 10 min at 4°C. The pellet was then re-suspended in respiration buffer B (250 mM Sucrose, 0.5 mM Na_2EDTA and 10 mM Tris), and an aliquot was used for protein determination. The remaining sample was then centrifuged at 6000*g* for 10 min at 4°C. The pellet was re-suspended in buffer A and centrifuged again at 6000*g* for 10 min at 4°C. The final crude mitochondrial pellet was re-suspended in MiR05 medium. Cerebrum was homogenized (1:10, w/v) in a respiration buffer C (0.32 M Sucrose, 1 mM EDTA-K^+ and 10 mM Tris–HCl, pH 7.4) at 500 r.p.m at 4°C in a glass–teflon homogenizer. The homogenate was centrifuged at 13 000*g* for 3 min at 4°C. S1 was kept on ice, and the pellet was re-suspended in 5 ml of buffer A and centrifuged at 13 000*g* for 3 min at 4°C. The subsequent supernatant (s2) was combined with s1 and centrifuged at 21 200*g* for 10 min at 4°C. Mitochondrial pellet of this step was re-suspended in 0.85 ml of extraction buffer A containing 15% Percoll, poured into ultracentrifuge tubes containing a Percoll gradient formed by 1 ml 40% Percoll and 1 ml 23% Percoll in buffer A and centrifuged at 63 000*g* for 30 min at 4°C. Pure mitochondria, corresponding to the fraction between 23 and 40% Percoll, were collected and washed twice with 1 ml of buffer A at 10 300*g* for 10 min at 4°C. Mitochondrial pellets were suspended in MIRO5 medium.

Mitochondrial respiration was measured by high-resolution respirometry using an OROBOROS Oxygraph-2k instrument at 37°C (42). Respiration in isolated mitochondria (0.09–0.1 mg protein/ml in cerebrum; 0.2–0.6 mg protein/ml in kidney; 0.01–0.03 mg of protein/ml in heart; 0.01–0.03 mg protein/ml in muscle) was measured in 2 ml MiR05 medium that was previously equilibrated in the chamber with air at 37°C and stirred at 750 r.p.m until a stable signal at air saturation was obtained. The sequence of measurements of respiratory states was as follows: initial state 2 was measured in the presence of 10 mM glutamate plus 2 mM malate (respiration through complex I) or 10 mM succinate + 2.5 μM rotenone (respiration through complex II); then, maximal mitochondrial respiration (state 3) was stimulated by adding 0.25 mM ADP, and state 4 was determined after state 3 in brain mitochondria, when all added ADP was consumed. In kidney, heart and skeletal muscle mitochondria, state 4 was measured after the addition of 3 μg/ml of oligomycin (state 4_o). State 3 and state 4 (or state 4_o) were expressed in pmol O_2/(s × mg protein). The RCR was calculated as the ratio of state 3 to state 4 (or state 4_o).

Histology and immunohistochemistry

Mice tissues were formalin fixed and paraffin embedded. Multiple sections (4 μm thickness) were deparaffinized with xylene and stained with H&E, Masson's TCM, PAS and LFB. Immunohistochemistry was carried out in the same sections, using the following primary antibodies: Glial fibrillary acidic protein or anti-GFAP (Millipore, MAB360), anti-oligodendrocytes (Millipore, MAB1580), Neuronal Class III β-tubulin anti-TUJ1 (Covance, MMS-435P), 8-OHdG (QED Bioscience, 12501) and 4-HNE (Alpha Diagnostic, HNE11-S) (42). The TUNEL method was performed in these samples using a commercial kit (ApopTag® Plus Peroxidase *in situ* Apoptosis Detection Kit, Code: S7101, Millipore) (43). Dako Animal Research Kit for mouse primary antibodies

(Dako Diagnóstico S.A., Spain) was used for the qualitative identification of antigens by light microscopy. Sections were examined at 40–400× with an OLYMPUS CX41 microscope, and the images were scanned under equal light conditions with the CELL A computer program.

Measurement of adenine nucleotides levels

Adenine nucleotides were separated and quantified by a Gilson HPLC-UV (44). Briefly, mice were sacrificed by cervical dislocation, and the whole animal was immediately frozen in liquid nitrogen. Tissues were quickly dissected on a cold plate, and 50 mg of each piece of tissue was homogenized in 500 μl of ice-cold 0.5 M perchloric acid, kept on ice for 10 min and then centrifuged at 25 000*g* for 10 min at 4°C. The pellets were stored at −80°C for protein measurement. The supernatants were neutralized with 50 μl of 4M K_2CO_3, kept on ice for 5 min and centrifuged at 12 000*g* for 10 min at 4°C. The resulting supernatants were kept at −80°C until injection into the HPLC. The mobile phase consisted of 100 mM potassium phosphate (pH 7), 1 mM tetrabutylammonium hydrogensulfate and 1.5% acetonitrile. Sample was run isocratically at a flow rate of 1.5 ml/min through a Kromasil® C18 (5 μm; 4.6 × 250 mm) reverse-phase column. The retention times for AMP, ADP and ATP were 3.4, 6.9, and 11.8 min, respectively. Standard curves for AMP, ADP and ATP were constructed with 15, 30 and 60 mM of each nucleotide. Absorbance of the samples was measured with an UV detector at 254 nm wavelength, and the concentration of each nucleotide in the samples was calculated based on the peak area. Adenine nucleotide levels were expressed in nmol/mg protein.

Determination of the metabolite profile in urine

Urine samples were collected for 24 h and analyzed in a BS-200 Clinical Chemistry Analyzer (Mindray Medical España S.L., Spain) at 37°C. The following colorimetric tests were performed: urea, magnesium, creatinine, glucose, calcium Arsenazo III and albumin, microalbumin (Linear Chemicals S.L., Spain).

Open-field test

To check spontaneous locomotor activity, we used the open-field test. The apparatus consisted of a square arena in a ground space of 25 × 25 × 25 cm. Walls were opaque, so the animals cannot see the room. Each mouse was placed in the center of the square arena, and its movement monitored through the video-tracking system SMART® (Panlab S.L., Spain) for 30 min after an adaption period of 30 min. (45). For each mouse, distance traveled (cm) and vertical rears (numbers) were quantified. Those tests were performed between 8 and 9 p.m. under red light exposure. At the end of each trial, any defecation was removed, and the apparatus was wiped with 70% ethanol.

Statistical analysis

Data are expressed as the mean ± SD of 520 experiments per group. Two-tailed Student's *t*-test was used to compare the mean between groups. A *P*-value of 0.05 was considered to be statistically significant.

SUPPLEMENTARY MATERIAL

Supplementary Material is available at *HMG* online.

ACKNOWLEDGEMENTS

We thank Dr Hekimi (McGill University, Canada) for providing the anti-Coq7 antibody. We are grateful to Dr Samuel Cantarero (Universidad de Granada), Dr Ana Nieto (Universidad de Granada) and Dr Manuel Pablo Olmos (AnaPath, Granada, Spain) for technical support. The authors appreciate the critical comments from Dr Catarina M. Quinzii (Columbia University).

Conflict of Interest statement. J.A.E. is a senior researcher of the CNIC. M.L.S. is a predoctoral fellow from the Consejería de Economía, Innovación, Ciencia y Empleo, Junta de Andalucía. A.G. is a predoctoral fellow from the Ministerio de Edicación y Ciencia, Spain. A.L. is a postdoctoral fellow from the Universidad de Granada.

FUNDING

This work was partially supported by grants from the Marie Curie International Reintegration Grant Programme (COQMITMEL-266691 to L.C.L.) within the seventh European Community Framework Programme, from Ministerio de Economía y Competitividad, Spain (SAF2009-08315 to L.C.L., SAF2009-08007 to J.A.E. and CSD2007-00020 to J.A.E.), from the Consejería de Economía, Innovación, Ciencia y Empleo, Junta de Andalucía (P10-CTS-6133 to L.C.L.) from the 'CEIBioTic' (20F12/1 to L.C.L.) and 'Incent' Programs of the Universidad de Granada, and from Comunidad Autónoma de Madrid (P2010/BMD-2402 to J.A.E.). The CNIC was supported by the MEC and the Pro-CNIC Foundation. R.A.P. and L.C.L. were supported by the 'Ramón y Cajal' National Programme, Ministerio de Economía y Competitividad, Spain (RYC-2011-07826 and RYC-2011-07643, respectively). J.A.G. and C.D. were supported by the Instituto de Salud Carlos III, Spain.

REFERENCES

1. Tran, U.C. and Clarke, C.F. (2007) Endogenous synthesis of coenzyme Q in eukaryotes. *Mitochondrion*, **7**(Suppl), S62–S71.
2. Johnson, A., Gin, P., Marbois, B.N., Hsieh, E.J., Wu, M., Barros, M.H., Clarke, C.F. and Tzagoloff, A. (2005) COQ9, a new gene required for the biosynthesis of coenzyme Q in *Saccharomyces cerevisiae*. *J. Biol. Chem.*, **280**, 31397–31404.
3. Lenaz, G. and Genova, M.L. (2007) Kinetics of integrated electron transfer in the mitochondrial respiratory chain: random collisions vs. solid state electron channeling. *Am. J. Physiol. Cell Physiol.*, **292**, C1221–C1239.
4. Acín-Pérez, R., Fernandez-Silva, P., Peleato, M.L., Perez-Martos, A. and Enriquez, J.A. (2008) Respiratory active mitochondrial supercomplexes. *Mol. Cell*, **32**, 529–539.

5. Schagger, H. (2001) Blue-native gels to isolate protein complexes from mitochondria. *Methods Cell Biol.*, **65**, 231–244.
6. Turunen, M., Olsson, J. and Dallner, G. (2004) Metabolism and function of coenzyme Q. *Biochim. Biophys. Acta*, **1660**, 171–199.
7. Emmanuele, V., Lopez, L.C., Berardo, A., Naini, A., Tadesse, S., Wen, B., D'Agostino, E., Solomon, M., DiMauro, S., Quinzii, C. *et al.* (2012) Heterogeneity of coenzyme Q10 deficiency: patient study and literature review. *Arch. Neurol.*, **69**, 978–983.
8. Rodriguez-Hernandez, A., Cordero, M.D., Salviati, L., Artuch, R., Pineda, M., Briones, P., Izquierdo, L.G., Cotan, D., Navas, P. and Sanchez-Alcazar, J.A. (2009) Coenzyme Q deficiency triggers mitochondria degradation by mitophagy. *Autophagy*, **5**, 19–32.
9. Lopez-Martin, J.M., Salviati, L., Trevisson, E., Montini, G., DiMauro, S., Quinzii, C., Hirano, M., Rodriguez-Hernandez, A., Cordero, M.D., Sanchez-Alcazar, J.A. *et al.* (2007) Missense mutation of the COQ2 gene causes defects of bioenergetics and de novo pyrimidine synthesis. *Hum. Mol. Genet.*, **16**, 1091–1097.
10. Quinzii, C.M., Lopez, L.C., Von-Moltke, J., Naini, A., Krishna, S., Schuelke, M., Salviati, L., Navas, P., DiMauro, S. and Hirano, M. (2008) Respiratory chain dysfunction and oxidative stress correlate with severity of primary CoQ10 deficiency. *FASEB J.*, **22**, 1874–1885.
11. Quinzii, C.M., Lopez, L.C., Gilkerson, R.W., Dorado, B., Coku, J., Naini, A.B., Lagier-Tourenne, C., Schuelke, M., Salviati, L., Carrozzo, R. *et al.* (2010) Reactive oxygen species, oxidative stress, and cell death correlate with level of CoQ10 deficiency. *FASEB J.*, **24**, 3733–3743.
12. Quinzii, C.M., Tadesse, S., Naini, A. and Hirano, M. (2012) Effects of inhibiting CoQ10 biosynthesis with 4-nitrobenzoate in human fibroblasts. *PLoS One*, **7**, e30606.
13. Hsieh, E.J., Gin, P., Gulmezian, M., Tran, U.C., Saiki, R., Marbois, B.N. and Clarke, C.F. (2007) *Saccharomyces cerevisiae* Coq9 polypeptide is a subunit of the mitochondrial coenzyme Q biosynthetic complex. *Arch. Biochem. Biophys.*, **463**, 19–26.
14. Duncan, A.J., Bitner-Glindzicz, M., Meunier, B., Costello, H., Hargreaves, I.P., Lopez, L.C., Hirano, M., Quinzii, C.M., Sadowski, M.I., Hardy, J. *et al.* (2009) A nonsense mutation in COQ9 causes autosomal-recessive neonatal-onset primary coenzyme Q10 deficiency: a potentially treatable form of mitochondrial disease. *Am. J. Hum. Genet.*, **84**, 558–566.
15. Nakai, D., Yuasa, S., Takahashi, M., Shimizu, T., Asaumi, S., Isono, K., Takao, T., Suzuki, Y., Kuroyanagi, H., Hirokawa, K. *et al.* (2001) Mouse homologue of coq7/clk-1, longevity gene in *Caenorhabditis elegans*, is essential for coenzyme Q synthesis, maintenance of mitochondrial integrity, and neurogenesis. *Biochem. Biophys. Res. Commun.*, **289**, 463–471.
16. Levavasseur, F., Miyadera, H., Sirois, J., Tremblay, M.L., Kita, K., Shoubridge, E. and Hekimi, S. (2001) Ubiquinone is necessary for mouse embryonic development but is not essential for mitochondrial respiration. *J. Biol. Chem.*, **276**, 46160–46164.
17. Kruse, S.E., Watt, W.C., Marcinek, D.J., Kapur, R.P., Schenkman, K.A. and Palmiter, R.D. (2008) Mice with mitochondrial complex I deficiency develop a fatal encephalomyopathy. *Cell Metab.*, **7**, 312–320.
18. Leong, D.W., Komen, J.C., Hewitt, C.A., Arnaud, E., McKenzie, M., Phipson, B., Bahlo, M., Laskowski, A., Kinkel, S.A., Davey, G.M. *et al.* (2012) Proteomic and metabolomic analyses of mitochondrial complex I-deficient mouse model generated by spontaneous B2 short interspersed nuclear element (SINE) insertion into NADH dehydrogenase (ubiquinone) Fe-S protein 4 (Ndufs4) gene. *J. Biol. Chem.*, **287**, 20652–20663.
19. Duberley, K.E., Abramov, A.Y., Chalasani, A., Heales, S.J., Rahman, S. and Hargreaves, I.P. (2012) Human neuronal coenzyme Q(10) deficiency results in global loss of mitochondrial respiratory chain activity, increased mitochondrial oxidative stress and reversal of ATP synthase activity: implications for pathogenesis and treatment. *J. Inherit. Metab. Dis.*, doi:10.1007/s10545-012-9511-0.
20. Xie, L.X., Ozeir, M., Tang, J.Y., Chen, J.Y., Kieffer-Jaquinod, S., Fontecave, M., Clarke, C.F. and Pierrel, F. (2012) Over-expression of the Coq8 kinase in Saccharomyces cerevisiae coq null mutants allows for accumulation of diagnostic intermediates of the Coenzyme Q6 biosynthetic pathway. *J. Biol. Chem.*, **287**, 23571–23581.
21. Stenmark, P., Grunler, J., Mattsson, J., Sindelar, P.J., Nordlund, P. and Berthold, D.A. (2001) A new member of the family of di-iron carboxylate proteins. Coq7 (clk-1), a membrane-bound hydroxylase involved in ubiquinone biosynthesis. *J. Biol. Chem.*, **276**, 33297–33300.
22. Heeringa, S.F., Chernin, G., Chaki, M., Zhou, W., Sloan, A.J., Ji, Z., Xie, L.X., Salviati, L., Hurd, T.W., Vega-Warner, V. *et al.* (2011) COQ6 mutations in human patients produce nephrotic syndrome with sensorineural deafness. *J. Clin. Invest.*, **121**, 2013–2024.
23. Genova, M.L. and Lenaz, G. (2011) New developments on the functions of coenzyme Q in mitochondria. *Biofactors*, **37**, 330–354.
24. Acín-Pérez, R., Bayona-Bafaluy, M.P., Fernandez-Silva, P., Moreno-Loshuertos, R., Perez-Martos, A., Bruno, C., Moraes, C.T. and Enriquez, J.A. (2004) Respiratory complex III is required to maintain complex I in mammalian mitochondria. *Mol. Cell*, **13**, 805–815.
25. Mootha, V.K., Bunkenborg, J., Olsen, J.V., Hjerrild, M., Wisniewski, J.R., Stahl, E., Bolouri, M.S., Ray, H.N., Sihag, S., Kamal, M. *et al.* (2003) Integrated analysis of protein composition, tissue diversity, and gene regulation in mouse mitochondria. *Cell*, **115**, 629–640.
26. Lapointe, J., Wang, Y., Bigras, E. and Hekimi, S. (2012) The submitochondrial distribution of ubiquinone affects respiration in long-lived Mclk1+/− mice. *J. Cell Biol.*, **199**, 215–224.
27. Lenaz, G., Daves, G.D. Jr. and Kfolkers, K. (1968) Organic structural specificity and sites of coenzyme Q in succinoxidase and DPNH-oxidase systems. *Arch. Biochem. Biophys.*, **123**, 539–550.
28. Miki, R., Saiki, R., Ozoe, Y. and Kawamukai, M. (2008) Comparison of a coq7 deletion mutant with other respiration-defective mutants in fission yeast. *FEBS J.*, **275**, 5309–5324.
29. Susin, S.A., Lorenzo, H.K., Zamzami, N., Marzo, I., Snow, B.E., Brothers, G.M., Mangion, J., Jacotot, E., Costantini, P., Loeffler, M. *et al.* (1999) Molecular characterization of mitochondrial apoptosis-inducing factor. *Nature*, **397**, 441–446.
30. Cregan, S.P., Fortin, A., MacLaurin, J.G., Callaghan, S.M., Cecconi, F., Yu, S.W., Dawson, T.M., Dawson, V.L., Park, D.S., Kroemer, G. *et al.* (2002) Apoptosis-inducing factor is involved in the regulation of caspase-independent neuronal cell death. *J. Cell Biol.*, **158**, 507–517.
31. Seiler, A., Schneider, M., Forster, H., Roth, S., Wirth, E.K., Culmsee, C., Plesnila, N., Kremmer, E., Radmark, O., Wurst, W. *et al.* (2008) Glutathione peroxidase 4 senses and translates oxidative stress into 12/15-lipoxygenase dependent- and AIF-mediated cell death. *Cell Metab.*, **8**, 237–248.
32. Lopez, L.C., Quinzii, C.M., Area, E., Naini, A., Rahman, S., Schuelke, M., Salviati, L., DiMauro, S. and Hirano, M. (2010) Treatment of CoQ(10) deficient fibroblasts with ubiquinone, CoQ analogs, and vitamin C: time- and compound-dependent effects. *PLoS One*, **5**, e11897.
33. Takahashi, M., Shimizu, T., Moriizumi, E. and Shirasawa, T. (2008) Clk-1 deficiency induces apoptosis associated with mitochondrial dysfunction in mouse embryos. *Mech. Ageing Dev.*, **129**, 291–298.
34. Lang-Rollin, I.C., Rideout, H.J., Noticewala, M. and Stefanis, L. (2003) Mechanisms of caspase-independent neuronal death: energy depletion and free radical generation. *J. Neurosci.*, **23**, 11015–11025.
35. Falk, M.J., Polyak, E., Zhang, Z., Peng, M., King, R., Maltzman, J.S., Okwuego, E., Horyn, O., Nakamaru-Ogiso, E., Ostrovsky, J. *et al.* (2011) Probucol ameliorates renal and metabolic sequelae of primary CoQ deficiency in Pdss2 mutant mice. *EMBO Mol. Med.*, **3**, 410–427.
36. Quinzii, C.M., Garone, C., Emmanuele, V., Tadesse, S., Krishna, S., Dorado, B. and Hirano, M. (2012) Tissue-specific oxidative stress and loss of mitochondria in CoQ-deficient Pdss2 mutant mice. *FASEB J.*, doi:0.1096/fj.12-209361.
37. Sofroniew, M.V. (2009) Molecular dissection of reactive astrogliosis and glial scar formation. *Trends Neurosci.*, **32**, 638–647.
38. Rodriguez, C.I., Buchholz, F., Galloway, J., Sequerra, R., Kasper, J., Ayala, R., Stewart, A.F. and Dymecki, S.M. (2000) High-efficiency deleter mice show that FLPe is an alternative to Cre-loxP. *Nat. Genet.*, **25**, 139–140.
39. Vestergren, R., Ullah, S., Cousins, I.T. and Berger, U. (2012) A matrix effect-free method for reliable quantification of perfluoroalkyl carboxylic acids and perfluoroalkane sulfonic acids at low parts per trillion levels in dietary samples. *J. Chromatogr. A*, **1237**, 64–71.
40. Fernandez-Vizarra, E., Lopez-Perez, M.J. and Enriquez, J.A. (2002) Isolation of biogenetically competent mitochondria from mammalian tissues and cultured cells. *Methods*, **26**, 292–297.
41. Zhang, M., Guo, R.X., Mo, L.Q., Liao, X.X., Li, W., Zhi, J.L., Sun, S.N., Wang, Y.L., Cui, Y., Liu, W. *et al.* (2009) Nuclear factor-kappaB mediates cytoprotection of hydrogen peroxide preconditioning against

apoptosis induced by oxidative stress in PC12 cells. *Clin. Exp. Pharmacol. Physiol.*, **36**, 304–311.
42. Lopez, L.C., Akman, H.O., Garcia-Cazorla, A., Dorado, B., Marti, R., Nishino, I., Tadesse, S., Pizzorno, G., Shungu, D., Bonilla, E. *et al.* (2009) Unbalanced deoxynucleotide pools cause mitochondrial DNA instability in thymidine phosphorylase deficient mice. *Hum. Mol. Genet.*, **18**, 714–722.
43. Suzuki, Y., Imada, T., Yamaguchi, I., Yoshitake, H., Sanada, H., Kashiwagi, T. and Takaba, K. (2012) Effects of prolonged water washing of tissue samples fixed in formalin on histological staining. *Biotech. Histochem.*, **87**, 241–248.
44. Manfredi, G., Yang, L., Gajewski, C.D. and Mattiazzi, M. (2002) Measurements of ATP in mammalian cells. *Methods*, **26**, 317–326.
45. Pallud, J., Haussler, U., Langlois, M., Hamelin, S., Devaux, B., Deransart, C. and Depaulis, A. (2011) Dentate gyrus and hilus transection blocks seizure propagation and granule cell dispersion in a mouse model for mesial temporal lobe epilepsy. *Hippocampus*, **21**, 334–343.